
This is an electronic reprint of the original article.
This reprint may differ from the original in pagination and typographic detail.

Yin, Yin; Roas-Escalona, Nelmary; Linder, Markus B.

Molecular Engineering of a Spider Silk and Mussel Foot Hybrid Protein Gives a Strong and Tough Biomimetic Adhesive

Published in:
Advanced Materials Interfaces

DOI:
[10.1002/admi.202300934](https://doi.org/10.1002/admi.202300934)

Published: 14/03/2024

Document Version
Publisher's PDF, also known as Version of record

Published under the following license:
CC BY

Please cite the original version:
Yin, Y., Roas-Escalona, N., & Linder, M. B. (2024). Molecular Engineering of a Spider Silk and Mussel Foot Hybrid Protein Gives a Strong and Tough Biomimetic Adhesive. *Advanced Materials Interfaces*, 11(8), Article 2300934. <https://doi.org/10.1002/admi.202300934>

This material is protected by copyright and other intellectual property rights, and duplication or sale of all or part of any of the repository collections is not permitted, except that material may be duplicated by you for your research use or educational purposes in electronic or print form. You must obtain permission for any other use. Electronic or print copies may not be offered, whether for sale or otherwise to anyone who is not an authorised user.

Molecular Engineering of a Spider Silk and Mussel Foot Hybrid Protein Gives a Strong and Tough Biomimetic Adhesive

Yin Yin, Nelmary Roas-Escalona, and Markus B. Linder*

High performance bio-based materials are an important part of future sustainable technology, and engineered proteins provide excellent possibilities as functional polymers. Adhesives are widely needed for composite materials and biomimetic structures. In biological adhesives, two features have emerged as especially interesting—the role of coacervation and the presence of 3,4-dihydroxyphenylalanine (DOPA). To study these, protein engineering is used to construct a hybrid silk-mussel foot protein (mfp) adhesive. Tyr residues in the purified mfp are oxidized to DOPA and an encoded SpyCatcher-Tag system allowed easy click-chemistry to couple silk and mfp and to study the parts separately. The combined silk-mfp protein have a strong tendency to coacervate. DOPA affected the properties of coacervates and increased adhesion by several ways of measuring. In lap shear testing, the combined mfp-silk protein is superior to any of the components studied separately. Coacervation is suggested to contribute to the adhesion of silk-mfp, and shows several features suggested to lead to the strength and toughness of natural adhesives. In the lap shear system, coacervation have a stronger overall effect on adhesion than the presence of DOPA. The results show that protein design provides a route toward high performance biosynthetic polymers and future sustainable materials.

from renewable resources in a sustainable way.^[1] Proteins show remarkable functions in nature, and a major challenge is to mimic these functions in a new context so that they in a feasible way can be used to make the materials we need for advanced or everyday applications. One material functionality that is of particular interest is adhesion. Adhesives form an increasingly central technology in manufacturing overall, for example, for creating lightweight structures,^[2–4] complex shapes,^[5,6] and enabling new production methods such as additive manufacturing.^[7] Importantly, these bio-based materials are formed in aqueous systems and do not require the use of organic solvents.^[8,9] By using adhesives for composites, we can for example upcycle and re-use natural fibers such as cellulose or find new uses for low-value fiber.^[10] Nanocomposites are also key approaches for unlocking the potential of components such as carbon nanotubes or graphene for high performance structures.^[11,12]

1. Introduction

Molecularly engineered proteins show a great potential for high-performance bio-based materials that are possible to produce

One unique potential of proteins for materials is that although they are large macromolecules, it is possible to engineer them with atomic detail. Protein engineering allows us to make structural and functional changes that are needed for taking them out of their biological context and developing them for use in new setups that fit our specific materials and processing needs. An example is the engineering of silk proteins to allow high-yield bacterial production and a technically feasible way of producing fiber with excellent properties.^[13] For adhesives, a source for bioinspiration are the adhesive systems originating from marine organisms. In particular the holdfast system of *Mytilus* species, that is, mussels, have served as biomimetic models.^[14,15] Their adhesive systems contain a number of proteins with specialized functions and are found in different regions of the adhesive plaques with specific roles and functions in both the sequence in which they are applied and in forming the final structural assemblies.^[15,16] In a simplified view, there are two features of these adhesive systems that have attracted especially wide attention. One is the extensive occurrence of the modified amino acid side chain 3,4-dihydroxyphenylalanine (DOPA)^[17] and the other is that the adhesive mussel foot proteins (mfps) undergo a

Y. Yin, N. Roas-Escalona, M. B. Linder
Department of Bioproducts and Biosystems, School of Chemical Engineering
Aalto University
Aalto FI-00076, Finland
E-mail: markus.linder@aalto.fi

Y. Yin, N. Roas-Escalona, M. B. Linder
Centre of Excellence in Life-Inspired Hybrid Materials (LIBER)
Aalto University
P.O. Box 16100, Aalto 00076, Finland

 The ORCID identification number(s) for the author(s) of this article can be found under <https://doi.org/10.1002/admi.202300934>

© 2024 The Authors. Advanced Materials Interfaces published by Wiley-VCH GmbH. This is an open access article under the terms of the [Creative Commons Attribution](https://creativecommons.org/licenses/by/4.0/) License, which permits use, distribution and reproduction in any medium, provided the original work is properly cited.

DOI: 10.1002/admi.202300934

liquid–liquid phase separation (LLPS)—also known as coacervation or condensation—as a step in their assembly from soluble protein into their final structures.^[18–21] DOPA is introduced as a post-translational modification by oxidization of Tyr-residues. The two hydroxyls of DOPA participate in metal chelation, π -cation interactions, and form hydrogen bonds with hydrophilic surfaces.^[22–26] At acidic pH the reactivity of DOPA is low, but at neutral or higher pH, DOPA is readily oxidized further into dopaquinone^[27] that participates in a wide range of reactions leading to, for example, crosslinking.^[28–31] These functions can be involved in both adhesion and cohesion in multiple ways, and it has been found that even the incorporation of DOPA in simple peptides markedly increase their adhesion to different surfaces.^[29,32] However, several studies have brought to attention that the natural system is more complex, with for example Lys residue side chains contributing to interactions and pointing out the important role of the overall structure of the proteins.^[33] The importance of coacervation for adhesion has been suggested since their initial observations, but a detailed understanding is still being formed.^[34] In parallel to these investigations, a wide understanding of coacervation as a mechanism for formation of biological assemblies and materials has emerged.^[28] Silk, the adhesive matrix of nacre, and other marine adhesive systems have been proposed to assemble through coacervation.^[28,35] A recurring theme for coacervating proteins—including silks and mfps—is that they contain intrinsically disordered regions (IDRs), that is, they do not take a specific 3D conformation in solution.^[36]

Coacervation can be driven by a number of different molecular interactions, and result in a concentrated phase with a high polymer (protein) concentration and a dilute phase.^[36] Some widely studied systems form complex coacervates in which two different polymers interact, typically by complementary charges. In biology, one-component systems are widespread, and in these identical polymer chains form interactions with each other. The water content in the coacervate is reduced and increased polymer–polymer interactions form. The molecular associations within the coacervates lead to a reduced conformational entropy of the protein chains—their order increases.^[37] Resulting bicontinuous internal structures in coacervates have been described.^[38] Protein association and possible formation of polymer entanglements are of particular interest as a route to enhanced cohesiveness in adhesives.^[39] Silk proteins have also attracted attention as adhesives. Silks form a large group of proteins that include ones from a wide range of insects and spiders. The spider-based silks show large variation, including adhesive functions. The exact molecular basis of the functional roles is not clear, as different variants of silk sequences show general adhesive properties. In particular, we have suggested previously that general features such as the interchain interactions in coacervates of also silks lead to adhesion.^[10]

In this work, we took a protein engineering approach to explore coacervation and DOPA as elements for designing novel biological adhesives. One problem that has hampered the use of recombinant mfps is that they are difficult to produce in full-length, and that engineered versions often suffer from poor solubility and low yield.^[40] Enzymatic in vitro modification of Tyr-residues to DOPA is well established, but the protocol involves many steps and can be difficult to perform if the protein is sen-

sitive to the conditions needed for the reaction.^[41] This led us to explore a hybrid approach in which relatively short parts of mfp1-protein were linked to a silk protein that previously has shown promising functionality as an adhesive.^[42] As the optimal production procedures for silk and mfp1 protein were not compatible, we utilized a system called SpyCatcher-SpyTag to covalently couple the components after they had been separately purified and mfp1 post-translationally modified.^[43] This molecular engineering approach in which components from widely different origins are combined—each bringing a specific functionality—allowed us to take a novel approach to understand and apply biological adhesives.

2. Results

2.1. Protein Production and Modification

Initial experiments showed that a mfp1 variant termed mfp1^{Tyr} having six tandem repeats of the consensus *M. edulis* mfp1 decapeptide AKPSYPPTYK^[44] fused with a SUMO tag SMT3^[45] at the N-terminal could be expressed in *E. coli* with yields of 80 mg l⁻¹ and was highly soluble. This “mfp1^{Tyr}”-protein contained a SpyTag^[43] for ligation and a His-tag for affinity purification. Its sequence and schematic structure are shown in **Figure 1**. Compared to other variants tested (Table S1, Supporting Information), it was found that the SMT3 domain gave increased yields and solubility.

Tyr residues in mfp1^{Tyr} were oxidized into DOPA by tyrosinase enzyme (Figure 1). Based on amino acid analysis, 65% of Tyr in the mfp1^{Tyr} were converted to DOPA, with the other 35%, remaining non-modified as Tyr. For clarity, we here denote the modified DOPA containing mfp1 protein, “mfp1^{DOPA}” to distinguish it from the nonmodified version mfp1^{Tyr}. The mfp1^{DOPA} version showed a slight smear on the SDS-PAGE (Figure S1, Supporting Information) compared to mfp1^{Tyr}. A similar smear for DOPA modified proteins has been reported earlier.^[44]

We made another protein—S-ADF3-S—which had a central part consisting of the repetitive region of the ADF3 spider silk protein^[46] and two flanking SpyCatcher002 (a variant of SpyCatcher)^[47] domains at each terminus (Figure 1). Production of S-ADF3-S resulted in a soluble protein with a yield of \approx 130 mg l⁻¹ of culture medium. The S-ADF3-S protein was purified from the periplasm of *E. coli* by heating cell lysate to precipitate endogenous proteins and performing a buffer exchange.

2.2. Formation of Coacervates

The SpyCatcher002-SpyTag ligation of both mfp1^{Tyr} and mfp1^{DOPA} to S-ADF3-S proceeded readily giving linked proteins here termed “S-ADF3-S:mfp1^{Tyr}” and “S-ADF3-S:mfp1^{DOPA}”. We mapped a range of different ratios of mfp1^{DOPA} and mfp1^{Tyr} to different amounts of S-ADF3-S and observed the effect on coacervation and linkage (Figure 2). In these experiments, 100 mM sodium acetate buffer at pH 5.0 was used. With molar excess or equimolar amounts of SpyTag to SpyCatcher002—taking into account that S-ADF3-S contains two SpyCatcher002 domains—coacervation was observed at a wide range of concentrations. With lower than equimolar amounts of SpyTag

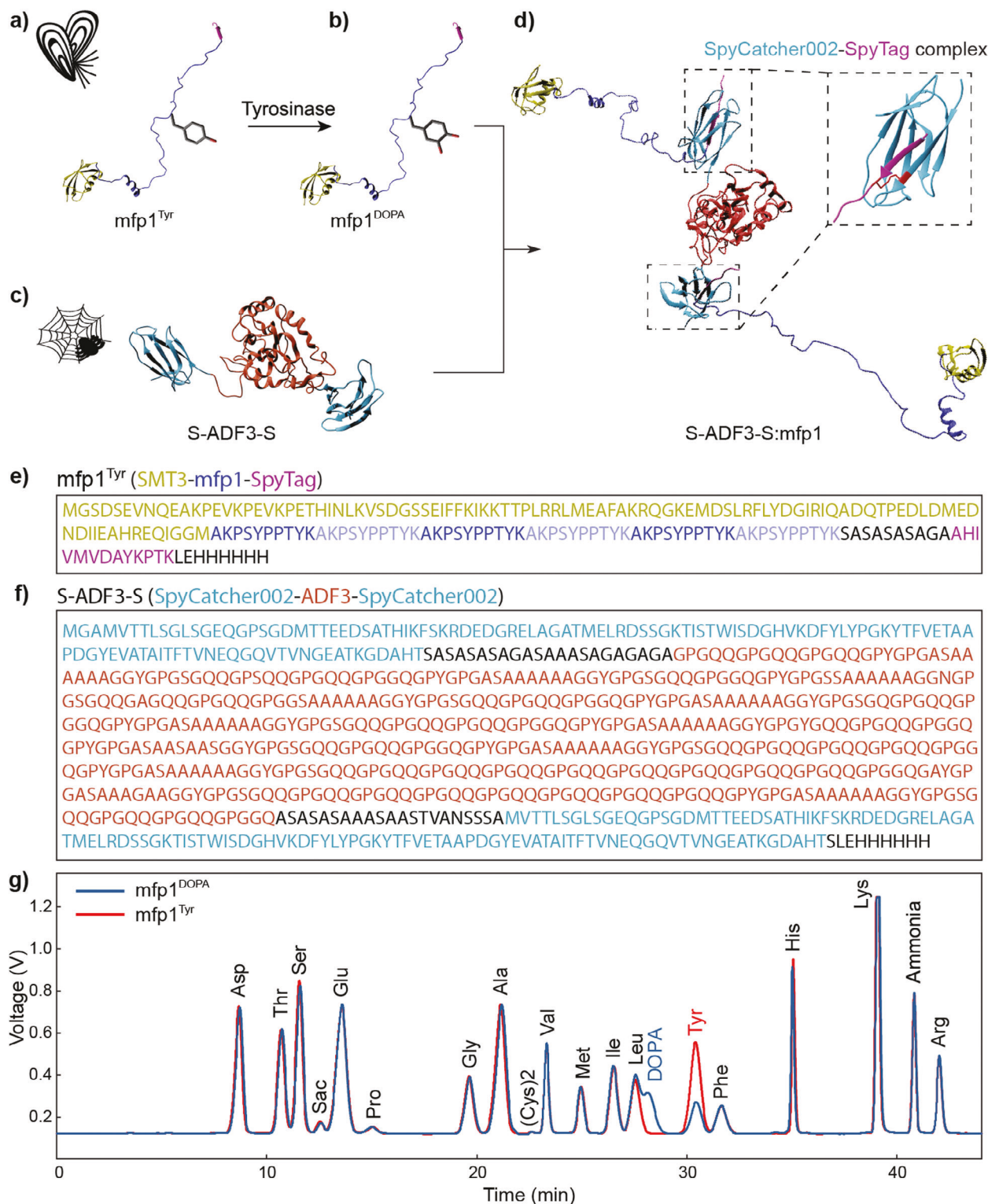


Figure 1. Strategy for assembling S-ADF3-S:mfp1 protein. a) Schematic structure of the $mfp1^{Tyr}$ protein which has three protein domains: a solubility tag SMT3 (based on PDB 1L2N), six tandem repeats of the decapeptide derived from *M. edulis* mfp1, and a SpyTag (based on PDB 4MLI). b) Schematic structure of $mfp1^{DOPA}$ in which part of the Tyr residues in $mfp1^{Tyr}$ are converted to DOPA. c) Schematic structure of the silk-like protein S-ADF3-S having a triblock structure with an intrinsically disordered silk sequence ADF3 as the mid-block and two SpyCatcher002 domains (PDB 4MLI) at each terminus. d) The S-ADF3-S:mfp1 protein was assembled by linking S-ADF3-S and $mfp1^{DOPA/Tyr}$ through the SpyCatcher002-SpyTag pair. e,f) The amino acid sequence of $mfp1^{Tyr}$ and S-ADF3-S. The colors correspond to the different domains in the proteins. g) Amino acid analysis of $mfp1^{DOPA}$ and $mfp1^{Tyr}$. In the $mfp1^{DOPA}$ sample, the amount of Tyr was lower than for $mfp1^{Tyr}$ and peak corresponding to DOPA peak appeared. The conversion of Tyr to DOPA was $\approx 65\%$.

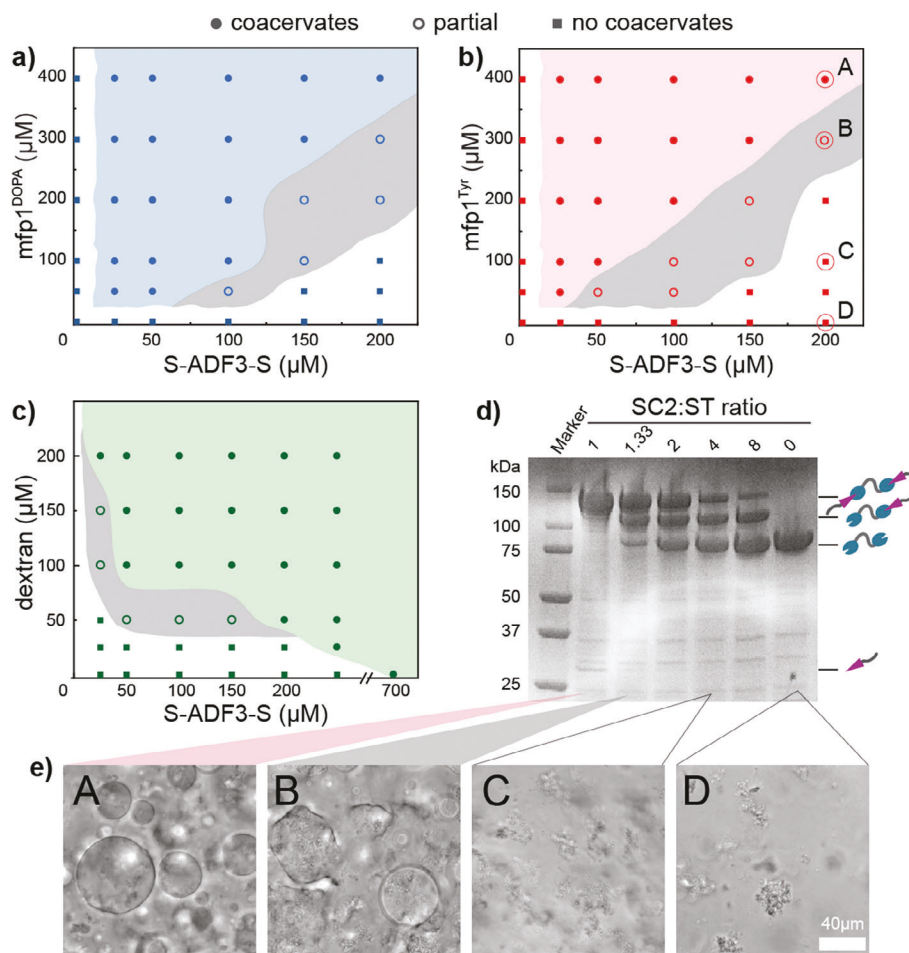


Figure 2. a) Phase diagram of S-ADF3-S with mfp1^{DOPA}. b) Phase diagram of S-ADF3-S with mfp1^{Tyr}. c) Phase diagram of S-ADF3-S with dextran 500. d) SDS-PAGE analysis of SpyCatcher002-SpyTag ligation with different SpyCatcher002:SpyTag (SC2:ST) ratios indicated in (b). The S-ADF3-S concentration was 200 μM, while the concentration of mfp1^{Tyr} varied from 0 to 400 μM. The proteins in each band are indicated on the side, and are from the bottom: mfp1^{Tyr}, S-ADF3-S, S-ADF3-S linked to one mfp1^{Tyr}, and S-ADF3-S linked to two mfp1^{Tyr}. e) Representative light microscopy images for A) coacervates, B) partial coacervates (coacervates mix with aggregates), C) no coacervates and D) S-ADF3-S protein alone. Scale bar: 40 μm.

to SpyCatcher002, we observed the formation of aggregates in combination with some coacervate droplets for both DOPA and Tyr versions. Plotting the results (Figure 2a,b) these combinations formed a region above the diagonal for excess mfp1^{DOPA} or mfp1^{Tyr} and below diagonal for excess S-ADF3-S. Coacervation was observed for both versions of the combined proteins at already 25 μM concentration of S-ADF3-S. This is a marked difference compared to the S-ADF3-S silk part alone, as it by itself did coacervate only at concentrations of 700 μM. Using dextran as a crowding agent, S-ADF3-S can form coacervates at much lower concentrations (Figure 2c).^[48]

2.3. General Properties of the Coacervates

We proceeded with a detailed characterization of the properties of coacervates formed by the both S-ADF3-S:mfp1^{DOPA} and S-ADF3-S:mfp1^{Tyr} proteins. A molar ratio of SpyCatcher002/SpyTag of 0.6 (80 μM S-ADF3-S and 267 μM mfp1^{Tyr}/mfp1^{DOPA}) was chosen for the characterization experiments,

as this combination showed clear coacervation behavior in the experiments above. The characterization of physical properties was done at pH 5 in 100 mM sodium acetate buffer. Using buffers with lower pH resulted in precipitation. Molecular diffusion within coacervates was studied using fluorescence recovery after photobleaching (FRAP) (Figure 3a). For FRAP, the S-ADF3-S molecule was labeled with a fluorophore (Oregon green) prior to the linking to mfp1^{DOPA} or mfp1^{Tyr}, allowing identical labeling of both variants. Using freshly prepared (1 h) samples, a diffusion coefficient (D) of $0.029 \mu\text{m}^2 \text{s}^{-1}$ was obtained for both variants, that is, no difference in D was observed. The mobile fraction was slightly larger for the Tyr than for the DOPA version ($82 \pm 0.9\%$ vs $76 \pm 1.8\%$). Over time, the nature of the coacervates changed—therefore measurements were also done 16 h after sample preparation. For samples at 16 h the mobile fraction for S-ADF3-S:mfp1^{Tyr} dropped only a little (to 68%), while for S-ADF3-S:mfp1^{DOPA} it was reduced markedly (to 32%) while D dropped for both versions ($0.021 \mu\text{m}^2 \text{s}^{-1}$ for S-ADF3-S:mfp1^{DOPA} and $0.019 \mu\text{m}^2 \text{s}^{-1}$ for S-ADF3-S:mfp1^{Tyr}) (Figure S2, Supporting Information). The change in mobile fraction for

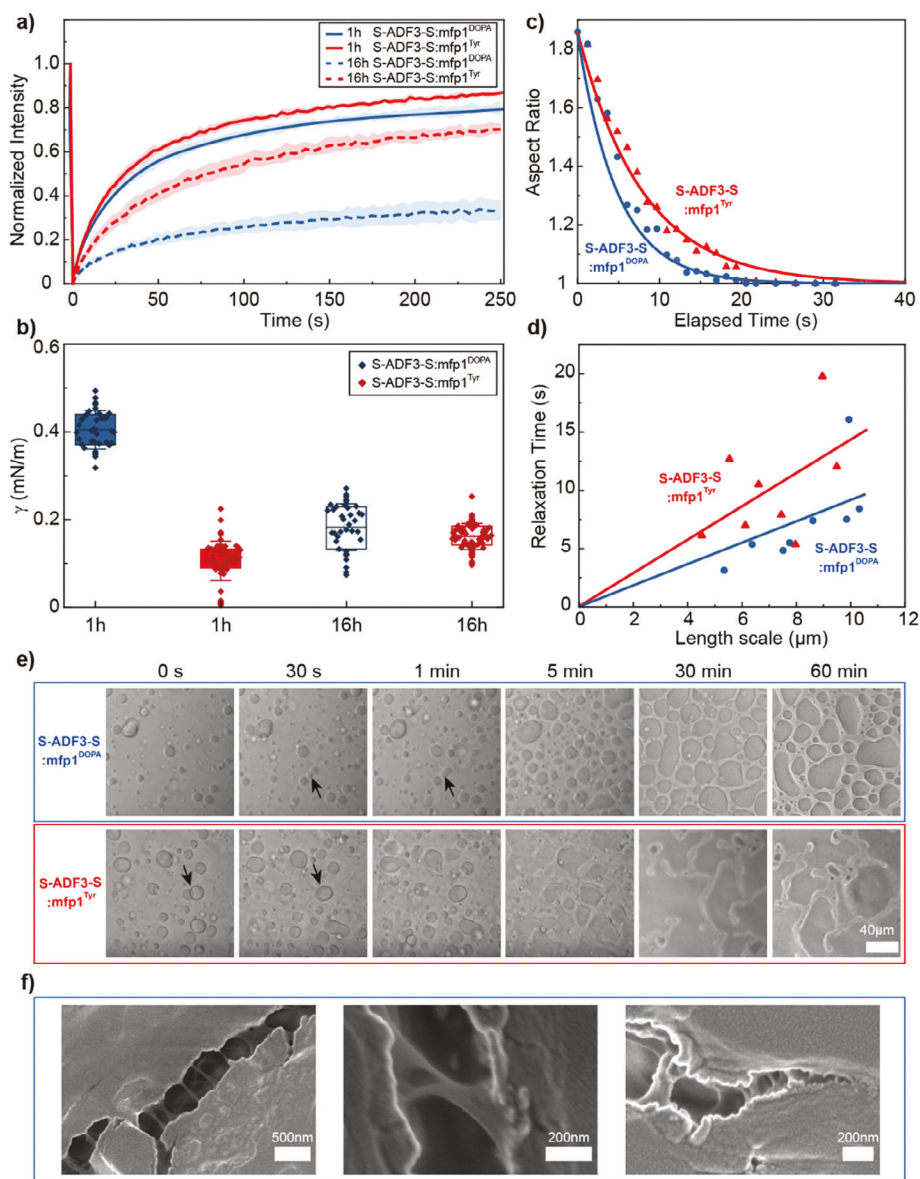


Figure 3. a) FRAP curves for the 1 and 16 h samples of S-ADF3-S:mfp1^{DOPA} and S-ADF3-S:mfp1^{Tyr} with coacervate diameters of 15–25 μm , $N = 5$. b) Interfacial tension of 1 and 16 h S-ADF3-S:mfp1^{DOPA} and S-ADF3-S:mfp1^{Tyr} coacervates estimated by glass colloidal probe AFM measurements. c) Analysis of fusion dynamics. The blue dots show the dynamics of an example fusion event of two 1 h S-ADF3-S:mfp1^{DOPA} coacervates and the blue line is the fitting curve. The red triangles show the slightly slower fusion dynamics of two 1 h S-ADF3-S:mfp1^{Tyr} coacervates with a red fitting curve. d) Plot of the relaxation time versus length from 1 h S-ADF3-S:mfp1^{DOPA} sample (blue dots) and 1 h S-ADF3-S:mfp1^{Tyr} sample (red triangles), $N = 8$. The blue and red lines are linear fits to the 1 h S-ADF3-S:mfp1^{DOPA} and 1 h S-ADF3-S:mfp1^{Tyr} data. e) Light microscopy images of coacervates morphologically change on a glass surface in response to the different time for 1 h S-ADF3-S:mfp1^{DOPA} and S-ADF3-S:mfp1^{Tyr} coacervates, separately. Arrows indicate the coalescence of two coacervates, scale bar 40 μm . f) Different magnifications of SEM images of cracks formed in 1 h S-ADF3-S:mfp1^{DOPA} coacervates when they were dried and teared. When teared, bridging ligaments are formed in the cracks.

the DOPA-version are in line with the expectation that at pH 5 a slow DOPA-mediated bridging and crosslinking in the structure occurred due to a slow oxidation of DOPA to dopaquinone. A slow oxidation of DOPA was also indicated by a slight brownish color developing due to dopaquinone formation.^[27] The drop in D for both versions show that molecular interactions develop in the mfp1^{Tyr} version as well. A slow viscosity increase is generally observed in ADF3-containing proteins over time.^[49]

We next studied the surface tension of the coacervates (Figure 3b) by colloidal probe-atomic force microscopy (AFM) capillary bridging. A marked difference between coacervates was found with S-ADF3-S:mfp1^{Tyr} showing significantly lower surface tension (γ) ($\approx 0.1 \text{ mN m}^{-1}$) than S-ADF3-S:mfp1^{DOPA} (0.4 mN m^{-1}) for 1 h samples. Over 16 h the surface tension of S-ADF3-S:mfp1^{DOPA} dropped to the same level of S-ADF3-S:mfp1^{Tyr} which did not change. For further exploring this finding, we recorded the time dependence of droplet coalescence for

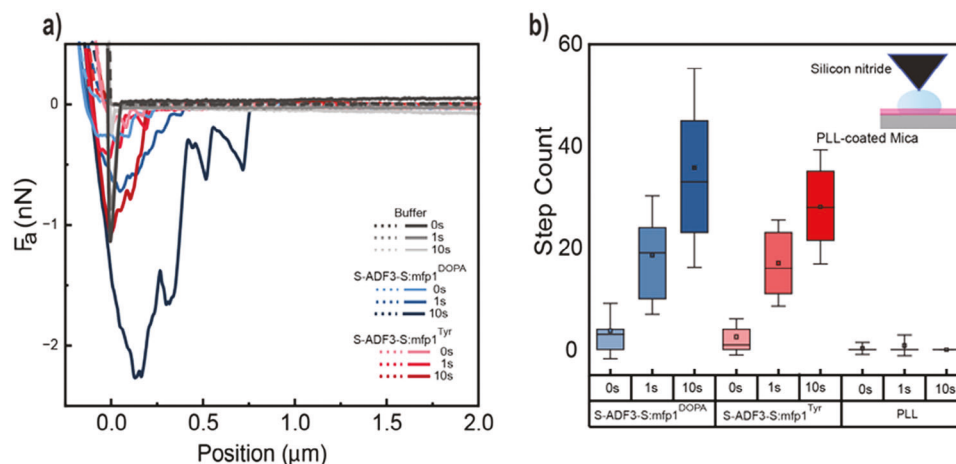


Figure 4. a) Typical force curves obtained in buffer and after absorbing S-ADF3-S:mfp1^{DOPA} and S-ADF3-S:mfp1^{Tyr}. Dashed and solid lines indicate data obtained during surface approach and retraction, respectively. All the curves correspond to random spots of the coated mica surface and coacervates. b) Average step counts corresponding to the multiple adhesives minima created during contact for absorbing S-ADF3-S:mfp1^{DOPA} and S-ADF3-S:mfp1^{Tyr} coacervates, and PLL.

1 h samples. From video recordings of droplet fusion events, the reduction of aspect ratio of the coalescing droplets was plotted against time, giving the relaxation time (τ) (Figure 3c). By combining data from droplets of different size and calculating the slope of a line fitted to the data gives the inverse capillary velocity (η/γ), that is, the viscosity η normalized by γ .^[50,51] This slope was lower—coalescence proceeded faster—for S-ADF3-S:mfp1^{DOPA} than for S-ADF3-S:mfp1^{Tyr}. Since viscosity and D are inversely proportional and since D was measured to be the same for both variants, it follows that γ is higher for S-ADF3-S:mfp1^{DOPA}, thereby confirming that the DOPA-modification does lead to an increase in surface tension. The surface tension difference could also be seen in how droplets adsorbed and spread on a glass surface (Figure 3e). S-ADF3-S:mfp1^{Tyr} showed a more spreading, that is, better surface wetting than S-ADF3-S:mfp1^{DOPA}.

As a means to study the internal structure of coacervate droplets, solutions were dried down on a parafilm support and then slightly stretched (Figure 3f). The stretching resulted in cracks in the protein films. In the cracks, there were clearly visible tear-out of ligaments which often formed bridges over the cracks. No qualitative differences ligament tear-out were observed between S-ADF3-S:mfp1^{DOPA} and S-ADF3-S:mfp1^{Tyr} (Figure 3f; Figure S3, Supporting Information).

2.4. Adhesive Properties by AFM

AFM was used initially for characterizing adhesive properties of the coacervates (molar ratio of SpyCatcher002/SpyTag of 0.6). Two different probes were used, a pyramidal silicon nitride probe and a spherical glass colloidal probe. We established an experimental setup where coacervates lay over muscovite mica having a polylysine (PLL) coating. The PLL coating resulted in a weak adherence of the coacervate droplets to the support material, enough to allow probing the coacervates with the AFM tip, but weak enough not to distort the droplets. To help understand

PLL adherence we measured zeta potentials (Table S3, Supporting Information). Coacervates have a slightly negative charge at pH 5, with values $\approx -0.41 \pm 0.06$ and -0.48 ± 0.4 mV for S-ADF3-S:mfp1^{DOPA} and S-ADF3-S:mfp1^{Tyr}, respectively. Some attractive electrostatic force between the PLL is expected. As above, experiments were done in sodium acetate buffer at pH 5.0 and with the same composition.

Probing S-ADF3-S:mfp1^{DOPA} and S-ADF3-S:mfp1^{Tyr} coacervates with the pyramidal tip gave force–distance curves with a sawtooth appearance (Figure 4a). Adhesive forces were higher—and showed a larger number of peaks which were at higher forces—for S-ADF3-S:mfp1^{DOPA} than for S-ADF3-S:mfp1^{Tyr}. The number of peaks were quantified as step-counts (Figure 4b), and show that the S-ADF3-S:mfp1^{DOPA} coacervates resulted in a higher number of adhesive contacts than S-ADF3-S:mfp1^{Tyr}. This stickiness may be due to more interactions between the tip and protein, or because S-ADF3-S:mfp1^{DOPA} condensates contain more numerous intramolecular crosslinks. The contact time had a marked effect on adhesive forces. Increasing contact time from 1 to 10 s (Figure 4a,b) resulted in roughly a doubling of adhesion force. As a reference measurement PLL-coated mica which gave adhesion forces of ≈ 1 nN and single minima at 10 s and 0.2 nN at instantaneous (0s adhesion).

Using the pyramidal silicon nitride tip, and probing the coacervate droplets, we found that S-ADF3-S:mfp1^{DOPA} coacervates did show higher adhesion forces than S-ADF3-S:mfp1^{Tyr} (Figure 5a). The adhesion force decreased with time, being almost equal between the samples after 16 h. Measuring the adhesion forces of regions surrounding the coacervate droplets we found similar adhesion forces to those of the coacervates (Figure 5b). A control sample of the PLL coated mica without proteins gave a force of 1.2 ± 0.22 nN, which was in the range observed for all protein samples except the freshly prepared S-ADF3-S:mfp1^{DOPA} samples. However, looking instead at the energy of adhesion—corresponding to the area under the force–distance curve—we do find that protein samples gave higher

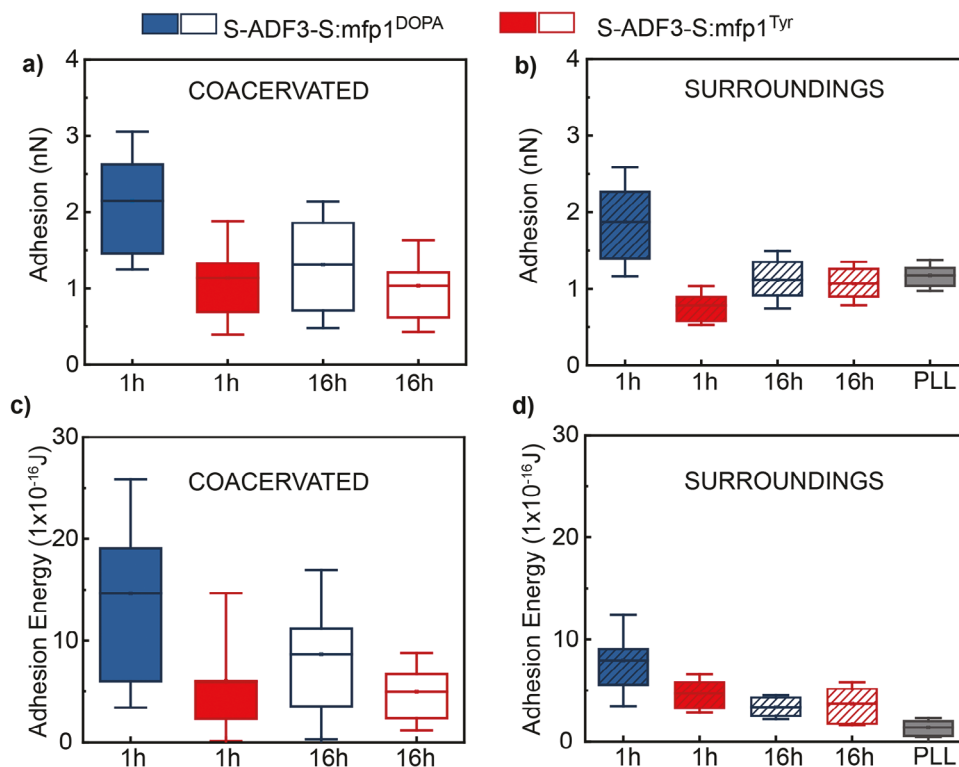


Figure 5. Adhesion force and adhesion energy of S-ADF3-S:mfp1^{DOPA} and S-ADF3-S:mfp1^{Tyr}. a) Comparison of the adhesion forces between the pyramidal tip and coacervates of S-ADF3-S:mfp1^{DOPA} and S-ADF3-S:mfp1^{Tyr} at 10 s of contact time for 1 and 16 h samples. Nine coacervate droplets were measured and for each, 16 random spots were chosen, and at every spot with five repetitions were made. b) Adhesion forces between pyramidal tip of the area surrounding coacervates at 1 and 16 h samples and 10 s of contact time. The plain PLL surface was also measured. The data represents the mean \pm SD of 9 areas surrounding the coacervates. In each area, 6 random points were chosen, and the forces curves were measured with five repetitions. c) As (a) but calculating the adhesion energy. d) As (b) but calculating the adhesion energy.

values (Figure 5c,d). The reason for this is that the multiple interactions due to the sawtooth retraction profile gives a larger integrated surface area. Protein samples measured in the regions surrounding the coacervates show higher adhesion energy than the PLL control indicating that protein was adsorbed to these regions. Aging of the sample did in all cases lead to a gradual lowering of adhesion (Figure 5a–d). The stiffness—Young’s modulus—of the S-ADF3-S:mfp1^{DOPA} coacervates was higher and increased over time more than it did for S-ADF3-S:mfp1^{Tyr} coacervates (Figure S4, Supporting Information).

We further investigated how the PLL-coating affects the system. Measurements were performed in a system with mica that was not coated and when both the silicon nitride tip and mica were coated with PLL. In the first case, the coacervates did not adhere sufficiently to the substrate making measurements practical. When PLL-coating the tip in addition to the support layer (Figure S5, Supporting Information), the adhesion values were below those obtained without coating on the tip. To probe the effect of an excess of mfp1 we used a mixture of 80 μM S-ADF3-S and 895 μM mfp1^{Tyr}/mfp1^{DOPA} (ratio 0.18). The adhesive properties of coacervates were not affected by the change in ratio (Figure S6, Supporting Information). An excess of S-ADF3-S did not result in analyzable coacervates.

Using AFM cantilevers with colloidal glass probes having a diameter of 5 μm at their ends allowed measuring normalized adhesion energies. Typical force curves for S-ADF3-

S:mfp1^{DOPA} and S-ADF3-S:mfp1^{Tyr} coacervates (molar ratio of SpyCatcher002/SpyTag of 0.6) at 10 s contact times are shown in Figure 6a. As with the pyramidal AFM-tips above, the contact time affected adhesion values strongly, and contact times of 1 s gave only \approx 40% of the adhesion compared to 10 s. The normalized adhesion energy ($E_{\text{ad}} = F_{\text{ad}}/1.5\pi R$) for the coacervates of the DOPA variant ($1.74 \pm 0.48 \text{ mJ m}^{-2}$) was clearly higher than for coacervates of the Tyr variant ($0.46 \pm 0.42 \text{ mJ m}^{-2}$) at 10 s contact time. Probing the regions around the coacervates gave much lower values.

Comparing the adhesion energy of S-ADF3-S:mfp1^{DOPA} and S-ADF3-S:mfp1^{Tyr} is affected by their differences in deformability, that is, stiffness, interfacial viscoelasticity, and surface energy. These factors differ between the two types of coacervates, and also change over time. In fresh samples both the surface energy and stiffness were higher for S-ADF3-S:mfp1^{DOPA} (Figure 3; Figure S4, Supporting Information). Since these factors lead to lower deformability, we can conclude that S-ADF3-S:mfp1^{DOPA} showed an enhanced adhesion compared S-ADF3-S:mfp1^{Tyr} (Figure S8, Supporting Information). For 16 h old samples the adhesion energy dropped for both S-ADF3-S:mfp1^{DOPA} and S-ADF3-S:mfp1^{Tyr} to a similar level. The oxidation of DOPA, increase in stiffness and viscosity together contributed to the decreased values, while the decrease in surface energy would be expected to counter the effect.

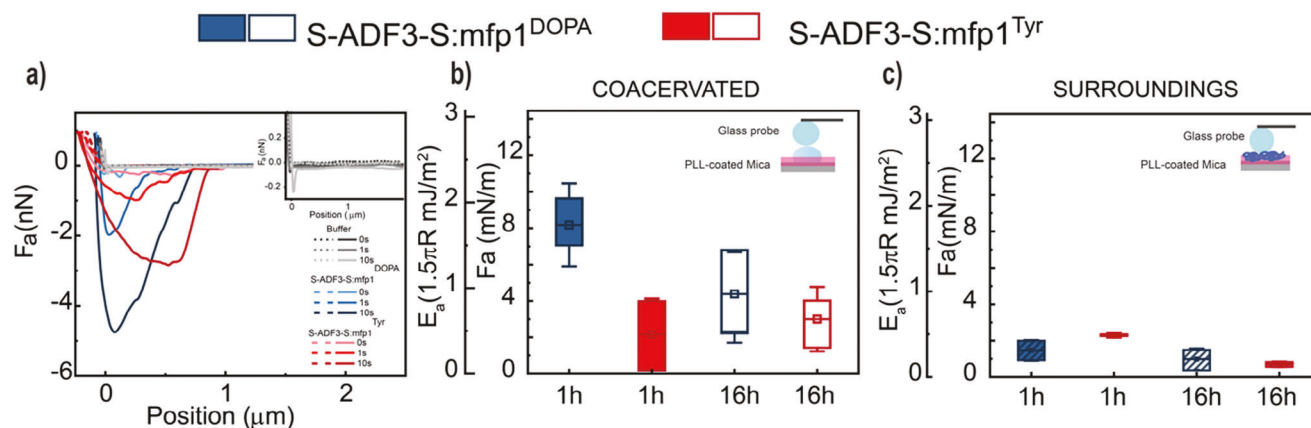


Figure 6. a) Typical force curves of S-ADF3-S:mfp1^{DOPA} and S-ADF3-S:mfp1^{Tyr} coacervates using colloidal glass probes ($D \approx 5 \mu\text{m}$). The dash and solid lines indicate data obtained during surface approach and retraction. The inset shows the force curves obtained with the buffer before absorbing the coacervates. b) A comparison at 10 s of contact time of the normalized adhesion force (F_{ad}/R) and normalized adhesion energy ($E_{ad} = F_{ad}/1.5\pi R$) between the glass probe and S-ADF3-S:mfp1^{DOPA} and S-ADF3-S:mfp1^{Tyr}, obtained for 1 and 16 h samples, respectively. The data represent the mean \pm SD of 10 coacervates. For each coacervate, 30 force curves were taken. c) A comparison of the normalized adhesion force and normalized adhesion energy between glass probe and S-ADF3-S:mfp1^{DOPA} and S-ADF3-S:mfp1^{Tyr} on areas surrounding coacervates for 1 and 16 h sample at 10 s contact time. The data represent the mean \pm SD of 10 areas. For each area, force curves were measured at 16 random points and five repetitions at every spot.

2.5. Adhesive Properties by Lap Shear Testing

We further studied the adhesive properties in lap shear tests. In order to understand the role of coacervation we prepared samples with both the assembled S-ADF3-S:mfp1^{DOPA} and S-ADF3-S:mfp1^{Tyr} as well as their components mfp1^{DOPA} and mfp1^{Tyr} and S-ADF3-S in separate experiments. We found that S-ADF3-S:mfp1^{DOPA} and S-ADF3-S:mfp1^{Tyr} both showed much higher lap shear strengths compared to the other samples but compared to each other they were largely similar (Figure 7). The free silk protein S-ADF3-S was close to mfp1^{DOPA}, and mfp1^{Tyr} had the lowest strength. Looking at the full load-displacement curves together with inspection of fracture areas gave further insight. The area under the load/displacement curve is a measure of work with the units of force times distance, and termed work of fracture. The displacement before fracture was clearly largest for S-ADF3-S:mfp1^{DOPA} and S-ADF3-S:mfp1^{Tyr}. The silk part S-ADF3-S by itself showed a higher work of fracture that mfp1^{DOPA} and especially mfp1^{Tyr}. Analyzing the fracture surfaces by microscopy we found that in all of the samples of S-ADF3-S:mfp1^{DOPA} and S-ADF3-S:mfp1^{Tyr} the adhesive was left on both surfaces, that is, they showed cohesive failure. Some also showed adherend failure—the glass substrate failed before the adhesive. For the three other samples the failure modes were mixed adhesive and cohesive.

3. Discussion

Our protein molecular engineering approach allowed to understand how two key concepts with biological adhesives—coacervation and the presence of DOPA—can be used in a biomimetic way. Both DOPA and coacervation show contributions to adhesion, but depending on how the adhesive system was set up, the contributions showed up differently. Forming the hybrid S-ADF3-S:mfp1 protein by the covalent SpyCatcher-SpyTag linkage triggers strong coacervation. On a general level,

coacervate formation is favored by multiple weak interactions between interacting protein chains. The detailed reasons for the high tendency for coacervation were not studied, but it is known that increased electrostatic interactions between chains and the length of these chains are expected contribute to the tendency for coacervation to occur.^[52] The calculated isoelectric points (pI) for S-ADF3-S and mfp1^{Tyr} are 4.77 and 9.19, respectively. At pH 5, S-ADF3-S is slightly negatively charged, and mfp1^{Tyr} is positively charged as also was confirmed by zeta potential experiments (Table S3, Supporting Information).

A key result here was that the hybrid S-ADF3-S:mfp1 adhesive coacervate performed very well in the lap shear test-setup with glass as the adherend. In this test the DOPA-version (S-ADF3-S:mfp1^{DOPA}) and the Tyr-version (S-ADF3-S:mfp1^{Tyr}) performed equally well. Both the strength of S-ADF3-S:mfp1 and the work of fracture—a measure of toughness—were clearly higher than for the constituent protein parts tested separately. The combination of high strength and toughness is a parameter that is often encountered in biological composite materials—and a key target of biomimetic materials research.^[7,53,54] It has been identified that factors that contribute to the combination of toughness and strength are the breaking of multiple weak bonds, stretching of entanglements in molecules, breaking of sacrificial bonds, and exposure of hidden lengths.^[55–57]

In coacervates, the protein molecules formed interactions between them as seen for example in that bridging ligaments formed in cracks when dried droplets were teared apart (Figure 3f; Figure S3, Supporting Information). Our observation is surprisingly similar to that shown for nacre and which has been suggested to form the basis of its toughness.^[54] In the AFM experiments with the pyramidal tip, the coacervated samples gave characteristic retraction patterns with multiple sawtooth interactions, indicating a connectivity that can come polymer interactions or multivalency. In AFM experiments the tip contact time was an important parameter. The effect of increase in adhesion with the length of contact time was expected and has been

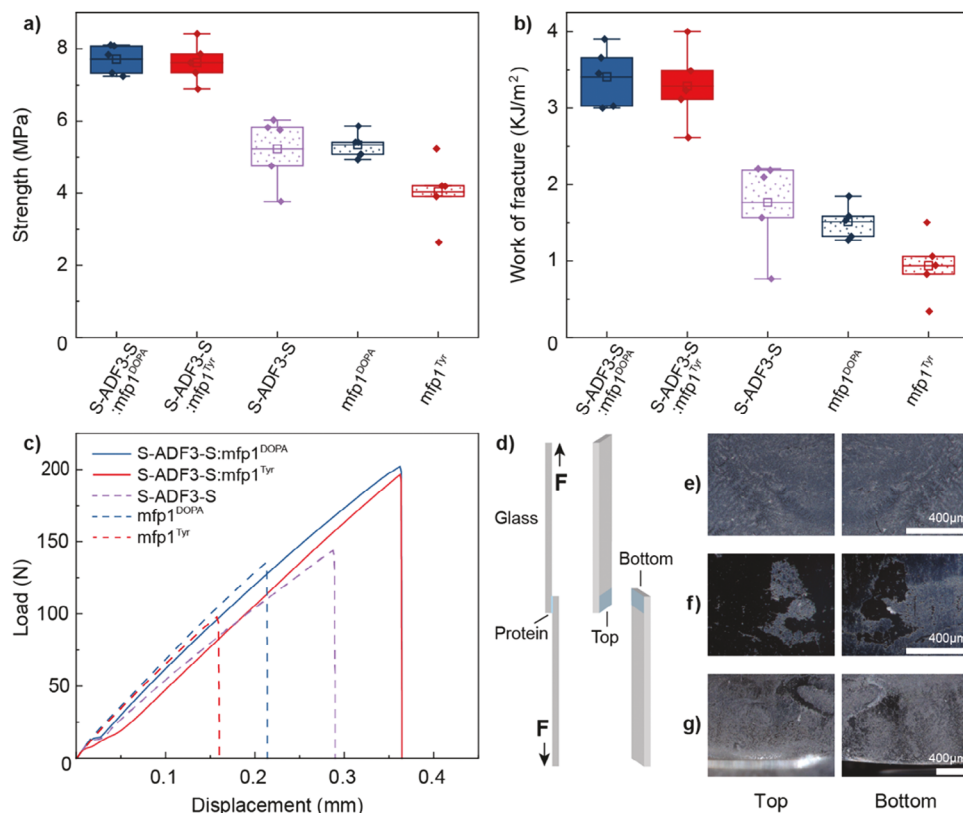


Figure 7. Comparison of the bulk adhesive strengths a) and work of fracture b) of the coacervated S-ADF3-S:mfp1^{DOPA} and S-ADF3-S:mfp1^{Tyr} individual proteins S-ADF3-S, mfp1^{DOPA} and mfp1^{Tyr}, $N = 5$. c) Representative load-displacement curves of each protein sample. d) Scheme of the lap shear test and the faces of the fracture surface. The digital microscopy images of the top and bottom fracture surfaces as the representative major failure mode: e) cohesive failure of adhesive, f) adhesion failure of adhesive/adherend interface and g) adherend failure. Scale bar = 400 μm .

described for in several cases using natural mussel proteins, for example, mfp5^[58] and affect absolute values for adhesion. S-ADF3-S:mfp1^{DOPA} gave higher adhesive forces even in the regions surrounding the coacervates (Figure 5b). We interpret this adhesion coming from non-coacervated protein from the dilute phase bound to the surface. That DOPA increases molecular adhesion in this fashion is a verification of previously published results.^[59–61] As the DOPA oxidized, the effect on adhesion decreased to baseline. The oxidation rate is dependent on pH. Here we used pH 5 which is the same as has been found for the plaque protein secretion in *M. edulis*.^[62,63] A lower pH has often been used to limit oxidation of mfps,^[58] but this was not practical in our study as it caused precipitation of S-ADF3-S:mfp1 proteins.

The effect of DOPA on coacervates is more debated, since even contradicting results have been obtained. Our findings agree with most other studies concluding that DOPA does not affect the phase separation in mfps.^[19,64–67] Individual reports suggests that DOPA does contribute to regulating phase separation in mfps.^[20] Looking at the effect of physical properties of DOPA on coacervates we found a pronounced effect on surface tension. A generality of this effect is possible as it was previously reported using SFA to study mfp-1 and hyaluronic acid (HA) that DOPA-containing coacervates had higher interfacial energy ($0.72 \pm 0.17 \text{ mJ m}^{-2}$) than coacervates lacking DOPA ($0.34 \pm 0.17 \text{ mJ m}^{-2}$).^[65] The increase in surface tension leads to a lower tendency to wet

surfaces it would be expected that in a natural system this would be a disadvantage (Figure 3e). This possible problem may have been overcome in some organisms by evolving special priming systems.^[68] However, in another study it was reported that complex coacervates formed by the recombinant adhesive protein (fp-151) and HA, the presence of DOPA did not change interfacial or other properties.^[64] DOPA has two hydroxyl groups and is more hydrophilic than Tyr. It is possible that a hydrophobic environment in coacervates forces molecular conformations at the droplet interface that result in the increased surface tension. DOPA also resulted in stiffer coacervates due to crosslinking. The stiffness increased over time.

Combining the understanding above we can present a model that explains the lap shear tests and suggests a further route for better engineered biosynthetic adhesives. By themselves in the lap shear tests both mfp1^{DOPA} and mfp1^{Tyr} showed brittle behavior and failed mostly at the interfaces. The mfp1^{DOPA} version performed better as its adhesion was stronger. However, it showed only little extension and failed in a brittle way at the interface. The strongly coacervating S-ADF3-S:mfp1^{DOPA} and S-ADF3-S:mfp1^{Tyr} showed a more extension before failure—they could sustain a larger deformation under tensile stress. The failure was cohesive or then the adherend failed before the adhesive. We also found that the silk unit S-ADF3-S by itself showed more extension than either mfp1^{DOPA} and mfp1^{Tyr} and showed also more mixed cohesive/interfacial failure. This is consistent

with its ability to coacervate to some extent even by itself at high concentrations (Figure 2c).

Extension of the bound layer helps distribute stress which explains why the interface is stable for the coacervating S-ADF3-S:mfp1^{DOPA} and S-ADF3-S:mfp1^{Tyr}.^[7,39,69] A distribution of stress decreases the risk of brittle failure at the interface. As the results show, adhesion to the surface was not the limiting factor for S-ADF3-S:mfp1^{DOPA} and S-ADF3-S:mfp1^{Tyr}. During coacervation of proteins, contact points—stickers—form between molecules. This results in a molecular network where protein molecules are associated with each other.^[70] Networks can be observed at the micro-scale as an internal network structure within coacervates.^[38] As studied more generally for proteins, coacervation as a step toward materials, therefore, affect both the formation process—as seen especially in fiber formation—and mechanical properties.^[71–73] We therefore propose that the ligament formation seen when stretching coacervates is an underlying property leading to extension of the protein in the lap shear tests, and thus higher toughness and strength.^[54] DOPA did not markedly affect this critical property of the adhesive in our system. In natural mfps this balance can be different, and therefore, DOPA can have a role of crosslinking and fine tuning of coacervate properties in addition to its interfacial binding function.

We demonstrated here that protein adhesives are a highly promising route toward designer biological materials combining performance and sustainable production methods. Based on our results we propose that the relation between molecular structure and coacervation and how the resulting molecular architecture affects the cohesion and extension mechanisms form crucial insights toward these new materials. For further developments of biological adhesives, it seems that a focus on the mechanisms of coacervation could hold more potential for improvements than what could be achieved by using DOPA-chemistry alone. Once we thoroughly understand how coacervation should be tuned for adhesion, we may find ways by which DOPA can further add to functionality.

4. Experimental Section

Cloning, Expression, and Purification of Proteins: Plasmid Construction. *S-ADF3-S Construct:* The DNA sequence encoding the engineered SpyCatcher002 (an E48K variant of SpyCatcher002^[47]) was codon optimized for expression in *E. coli* and ordered from GeneArt by gene synthesis (Thermo Fisher Scientific). S-ADF3-S was constructed by replacing the CBM domains from previously described CBM-ADF3-CBM construct^[72] with SpyCatcher002 domains by conventional restriction-ligation cloning with *NcoI* and *NheI* sites at N-terminal and *EcoRI* and *XhoI* sites at C-terminal.

For the mfp1^{Tyr} construct, a DNA sequence of six repeats of AKPSYPPTYK^[44] from mfp1 was codon optimized and synthesized by GeneArt (Thermo Fisher Scientific) for expression in *E. coli*. The genes for SMT3 were amplified by PCR with introduced compatible overhangs for Golden Gate cloning. The sequence of SpyTag and the linker (SASASASAGA) were ordered from Eurofins as oligos. Fusion constructs were made by seamless Golden Gate cloning with *BsaI* sites. The pE-28a (+) (kanR) (Novagen) expression vector in frame with the C-terminal 6xHis-tag sequence for was used. TOP10 strain was used as a cloning strain. All constructs were verified by sequencing.

Protein Expression: BL21(DE3) was used as expression strain for both constructs. Magic Media *E. coli* expression medium (Thermo Fisher Scientific) were used for protein expression according to the protocol from

the manufacturer with some changes. In short, one colony from freshly grown overnight LB-plate was picked and inoculated into 100 ml LB-media supplemented with 50 μM ml⁻¹ kanamycin. The culture was grown at 37°C, 220 rpm, overnight. The entire 100 ml start culture added into 900 ml Magic Media containing 50 μg ml⁻¹ kanamycin in two 2 l flasks. Protein was expressed at 30°C, 220 rpm, 24 h. The whole purification process was carried out at room temperature for S-ADF3-S and at 4°C for mfp1^{Tyr}. Cells were collected by centrifugation at 5000 rpm, 20 min. Cells were lysed in lysis buffer (5 ml g⁻¹) and incubated on a roller shaker for 1 to 3 h. For S-ADF3-S, the lysis buffer was 50 mM Tris-HCl pH 7.4, 100 mM NaCl, 1 mg ml⁻¹ lysozyme, 10 μg ml⁻¹ DNaseI, 3 mM MgCl₂, 1 tablet of protease inhibitor cocktail in 100 ml buffer. For mfp1^{Tyr} it was 50 mM sodium phosphate pH 8.0, 300 mM NaCl, 5 mM imidazole, 1 mg ml⁻¹ lysozyme, 10 μg ml⁻¹ DNaseI, 3 mM MgCl₂, 1 tablet of protease inhibitor cocktail in 100 ml buffer. An Emulsiflex homogenizer (AVESTIN-Emulsiflex-C3) was used for cell disruption. Cell debris was removed by centrifugation at 12 000 rpm for 20 min and followed by purification using heat treatment for S-ADF3-S and immobilized metal affinity chromatography (IMAC) for mfp1^{Tyr}. For S-ADF3-S: the lysis supernatant was heated at 70°C for 30 min and centrifuged at 12 000 rpm for 20 min to precipitate endogenous proteins which were not thermostable. Desalting of the protein samples was carried out with Econo-Pac 10DG desalting prepacked gravity flow columns (Bio-Rad). Concentration of protein samples was carried out with Vivaspin 20, 30 kDa MWCO centrifugal concentrators (Sartorius). Aliquots were frozen in liquid nitrogen and stored at -80°C for future use. For mfp1^{Tyr}, lysed supernatant was purified by using His-Trap FF crude columns (GE Healthcare Life Sciences) connected to an ÄKTA-Pure fast protein liquid chromatography system. The binding buffer contained 50 mM sodium phosphate, 300 mM NaCl and 5 mM imidazole, pH 8.0. The elution buffer contained 50 mM sodium phosphate, 300 mM NaCl and 250 mM imidazole, pH 8.0. For desalting of mfp1^{Tyr} SnakeSkin Dialysis Tubing, 3.5K MWCO, 22 mm (Thermo Scientific) was used against deionized water. Samples were stored at -80°C for future use.

Modification of Tyrosine Residues: To convert Tyr residues of the purified mfp1^{Tyr} to DOPA to mfp1^{DOPA}, commercially available mushroom tyrosinase (Sigma–Aldrich) was used for modification. The reaction system contained 100U ml⁻¹ mushroom tyrosinase, 100 mM HEPES at pH 7.8, 20 mM boric acid at pH 7, 50 mM ascorbic acid and the protein concentration was \approx 0.5 mg ml⁻¹. The reaction was carried at 25°C for 6 h with shaking and aeration. As a control mfp1^{Tyr} underwent the same process except without any mushroom tyrosinase added in the reaction system. After modification, the samples were dialyzed in 5% acetic acid by using SnakeSkin Dialysis Tubing, 3.5K MWCO, 22 mm (Thermo Scientific) and followed by lyophilization and were then stored at -80°C for future use.

Amino Acid Analysis: The conversion rate from Tyr to DOPA was determined by amino acid analysis, which a ninhydrin-based amino acid analyzer (Sykam) was used. Protein samples were hydrolyzed in 1 ml of 6 M HCl with 0.1% phenol, in vacuum at 110°C for 24 h. After evaporation, the hydrolyzed products were dissolved in 120 mM sodium citrate buffer at pH 3.45 and injected into the amino acid analyzer.

Sodium Dodecyl Sulfate-Polyacrylamide Gel Electrophoresis (SDS-PAGE): SDS-PAGE was used to check the protein production and SpyCatcher-SpyTag ligation reaction. A 4%–20% precast gel (Bio-Rad) was used and 10 μl of each sample was loaded on the gel.

Light Microscopy: Coacervate formation was initiated by mixing S-ADF3-S and mfp1^{DOPA} or mfp1^{Tyr} at different concentrations to form S-ADF3-S:mfp1^{DOPA} or S-ADF3-S:mfp1^{Tyr} proteins through SpyCatcher-SpyTag ligation. The ligation was carried out at 100 mM sodium acetate, at pH 5. For the phase diagram, S-ADF3-S, mfp1^{DOPA}, mfp1^{Tyr} and dextran (500 kDa) solutions were prepared beforehand in several different concentrations in 100 mM sodium acetate, at pH 5 and then mixed in 1:1 volume ratio to reach the final concentrations. The reaction of S-ADF3-S and mfp1^{DOPA} or mfp1^{Tyr} was either freshly mixed (1 h sample) or incubated for 16 h at room temperature for later use. The coacervate formation was visually inspected by Axio Observer inverted light microscope (Zeiss). Imaging was done with and without a cover glass to observe the coacervates.

For characterization of coacervates, S-ADF3-S and mfp1^{DOPA} or mfp1^{Tyr} were freshly mixed with a molar ratio of 0.3:1 (SC2:ST = 0.6) at room temperature. Then 5 μl of the mixture solution placed on a petri dish with a glass surface to observe morphological change and coalescence by microscope with time. According to the coalescence experiments, the inverse capillary velocity can be determined. The aspect ratio (A.R.) of the protein droplets was determined by fitting an ellipse to the coacervate contour and calculating the aspect ratio according to Equation (1) where l_{long} and l_{short} are the major long and short axes of the ellipse. For analysis of the merging droplets, the time evolution of this aspect ratio was fitted to function (2), where t is time, τ is the characteristic relaxation time, and $A.R._0$ is the initial aspect ratio. The length scale was defined as a geometric mean by using Equation (3). Plots of τ versus l were fitted to a line, to determine the inverse capillary velocity (η/γ) according to Equation (4).

$$A.R. = \frac{l_{\text{long}}}{l_{\text{short}}} \quad (1)$$

$$A.R. = 1 + (A.R._0 - 1) \cdot e^{-\frac{t}{\tau}} \quad (2)$$

$$l = \sqrt{(l_{\text{long}(t=0)} - l_{\text{short}(t=0)}) \cdot l_{\text{short}(t=0)}} \quad (3)$$

$$\frac{\tau}{l} = \frac{\eta}{\gamma} \quad (4)$$

Fluorescence Recovery after Photobleaching (FRAP): FRAP was performed on a Leica SP8 STED confocal microscope equipped with FRAP booster with a 63x/1.2 water objective. Surface-exposed lysine residues in S-ADF3-S selectively labeled using Oregon Green 488 (carboxylic acid, succinimidyl ester, 6-isomer), according to instructions provided by the distributor (Thermo Fisher). Recovery of a bleached spot of radius $r = 1 \mu\text{m}$ inside coacervates of diameter $\approx 20 \mu\text{m}$ were recorded. Intensity traces were corrected for photobleaching, normalized, and fit to the Equation (5), where A is the mobile fraction and τ is the recovery timescale. According to τ , the diffusion coefficient D can be determined by Equation (6).

$$f(t) = A(1 - e^{-t/\tau}) \quad (5)$$

$$D \approx r^2/\tau \quad (6)$$

Scanning Electron Microscopy (SEM): SEM imaging was implemented by using a Zeiss Sigma VP-SEM operated at 1.5 kV with a InLens detector. Samples were prepared by pipetting 5 μL of freshly mixed the S-ADF3-S:mfp1^{DOPA}, S-ADF3-S:mfp1^{Tyr} at a ratio of 0.3:1 (SC2:ST = 0.6) at room temperature on a piece of parafilm. When the protein solution was almost dried out, the parafilm was stretched. Both samples were coated with 7 nm platinum/palladium.

Atomic Force Microscopy (AFM): The coacervate adhesion was evaluated by AFM in constant-force mode and the colloidal probe technique.^[74] First, 50 μl of the coacervate solution was deposited and absorbed on PLL-coated mica under sodium acetate buffer pH 5. After 30 min, 20 μl of the sample were extracted and diluted with 100 μl of buffer solution to remove the excess coacervates that did not adhere to the substrate. Then we measured the temporal adhesion between Si₃N₄ quadratic pyramid tip and coacervates that were bound to PLL coated mica. Both quantitative imaging as force continuous measurement modes were applied. AFM force measurements were performed at room temperature in a buffered solution of 100 mM sodium acetate (pH 5) using JPK NanoWizard AFM system. The adhesion of S-ADF3-S:mfp1^{DOPA} and S-ADF3-S:mfp1^{Tyr} (SC2:ST = 0.6) was evaluated. Force curves were measured at a rate of 2–3 Hz, using cantilevers with calibrated spring constants between 0.04 and 0.06 N m⁻¹.

A glass sphere probe (CP-qp-CONT-BSG, $D \approx 5 \mu\text{m}$) was used to measure the asymmetric adhesion of coacervates, which pre-bound firmly to mica and bound temporarily to the AFM tip surface during measurement. The force curves were measured at a rate of 4 Hz and calibrated spring

constant between 0.06 and 0.15 N m⁻¹. JPKSPM data analysis software and Origin 2020 software (OriginLab Corporation) were used to analyze the image and force curves processing. Data are presented as mean \pm SD. The value of SD for quadratic pyramid tip and coacervate probe was obtained from 10 coacervates. It was taken 20–25 points within coacervate with 5 repetitions giving a total of 100–125 force curves for each coacervate. We also applied control tests for each measurement by directly measuring adhesion on a clean mica surface under the same conditions. The measured adhesion forces (F_{ad}) were taken at the point of maximum force on the retraction curves and were related to the adhesion energy per area (E_{ad}) according to the Johnson–Kendall–Roberts theory for deformable surfaces.^[75,76] The adhesion energy per unit of area is given by $E_{\text{ad}} = F_{\text{ad}}/2\pi R$ for rigid surfaces and $E_{\text{ad}} = F_{\text{ad}}/1.5\pi R$ for soft deformable surfaces with firm adhesive contact. Where $R = \frac{R_1 R_2}{R_1 + R_2}$, if R_2 is a flat surface or large sphere so $R_2 \gg R_1$ and we have $R = R_1$.

Interfacial Tension: The interfacial tension was determined using a colloidal probe atomic force microscopy (CP-AFM) from spectroscopy experiments. Force curves were measured on coacervates with 20–30 repetitions at 10s of contact time. The interfacial tension was calculated from capillary adhesion force at zero separation, which is valid close to saturation. The capillary forces measured in the CP-AFM setup for this system did not show signs of hysteresis. The hysteresis-free force-distance measurements allowed us to use equilibrium thermodynamics to analyze the results. By the method of Sprakel et al.,^[77,78] when the capillary bridge is near its binodal concentration, meaning that saturation conditions apply, the attractive force, extrapolated to zero separation follows the equation: $\lim_{\mu \rightarrow \mu^*} F_h = 0 = -2\pi R \gamma \cos(\theta)$, where R is the radius of the spherical probe, θ is the contact angle at the three-phase contact line. The above extrapolation was carried out by plotting all the force curves simultaneously for each coacervate and using the region of attractive force to extrapolate linearly to zero separation, using MatLab, as shown in Figure S8 (Supporting Information). Data are presented as mean \pm SD. Values for SD were obtained from the data of 4 condensate droplets \times 25 force curves.

Zeta Potential Measurements: Zeta potential of protein solutions (0.1 mg ml⁻¹) were obtained using the Malvern Nano ZS, which is calibrated using the Malvern Zeta Potential transfer standard. The proteins were solubilized in 100 mM sodium acetate buffer at pH 5.

Lap Shear Tests: The lap shear testing was performed using glass adherends (50 \times 5 \times 2 mm) to evaluate the bulk adhesive strength. The adherends were soaking for 3 h in a soap solution, rinsing with ethanol and then deionized water, and dried overnight in air at room temperature. The S-ADF3-S (50.4 mg ml⁻¹) and mfp1^{DOPA/Tyr} (49.5 mg ml⁻¹) were prepared separately in 100 mM sodium acetate, at pH 5 as the stock solutions. For the coacervate samples, 2 μl of S-ADF3-S was spread on the adherend followed by 2 μl of mfp1^{DOPA} or mfp1^{Tyr}, where the ratio of S-ADF3-S to mfp1^{DOPA/Tyr} was 0.3:1 (SC2:ST = 0.6). The protein solutions were mixed using a pipette. For the individual protein (non-coacervated) samples, 4 μl of S-ADF3-S, mfp1^{DOPA} or mfp1^{Tyr} was spread on the adherend by a pipette. For all the samples, the second adherend was placed after 5 min of the protein deposition. The adherends were overlapped with an area of 5 \times 5 mm and fixed by a clamp to keep the good contact. The adherends were cured for 18 h at room temperature before measurement. The samples were tested on an Instron 5567 universal testing machine with a 1000 N load cell and a loading rate of 1.5 mm min⁻¹. Load–displacement curves were recorded during the measurements. The bulk adhesive strength was determined by the maximum failure force divided by the overlap area and work of fracture was calculated as the area under the entire load–displacement curve. Each measurement was tested five times and the averaged data and standard deviations are reported. After measurements, the failure surfaces were visualized by a digital microscope.

Supporting Information

Supporting Information is available from the Wiley Online Library or from the author.

Acknowledgements

The authors acknowledge the light microscopy unit of the institute of biotechnology, University of Helsinki for providing facilities and support for FRAP experiments and OtaNano Nanomicroscopy center for access to their SEM facility. The authors thank Mohammad Mubinur Rahman for his expertise in optimizing the method for modification of tyrosine residues and Roosa Ilvonen for her contribution in protein expression and purification. They authors thank Juan Valle Delgado for his guidance in the characterization of coacervate adhesion by AFM. This work was funded by the Research Council of Finland (formerly the Academy of Finland) through projects # 317395, #326345, #346105 the Center of Excellence Program (2022-2029) in Life-Inspired Hybrid Materials (LIBER), and by the Novo Nordisk Foundation (NNF20OC0061306).

Conflict of Interest

The authors declare no conflict of interest.

Data Availability Statement

The data that support the findings of this study are available from the corresponding author upon reasonable request.

Keywords

adhesive, biomimetics, coacervation, condensation, liquid–liquid phase separation

Received: November 4, 2023
Revised: December 13, 2023
Published online: January 2, 2024

- [1] A. Miserez, J. Yu, P. Mohammadi, *Chem. Rev.* **2023**, 123, 2049.
- [2] K. G. Hoffmann, K. Haag, J. Müssig, *Mater. Des.* **2021**, 212, 110281.
- [3] A. Walther, I. Bjurhager, J. M. Malho, J. Pere, J. Ruokolainen, L. A. Berglund, O. Ikkala, *Nano Lett.* **2010**, 10, 2742.
- [4] N. Mittal, R. Jansson, M. Widhe, T. Benselfelt, K. M. O. Håkansson, F. Lundell, M. Hedhammar, L. D. Söderberg, *ACS Nano* **2017**, 11, 5148.
- [5] Z. Xiao, Q. Zhao, Y. Niu, D. Zhao, *Soft Matter* **2022**, 18, 3447.
- [6] P. Dwivedi, K. Singh, K. Chaudhary, R. Mangal, *ACS Appl. Polym. Mater.* **2022**, 4, 4588.
- [7] G. Raos, B. Zappone, *Macromolecules* **2021**, 54, 10617.
- [8] Y. Yang, X. Song, X. Li, Z. Chen, C. Zhou, Q. Zhou, Y. Chen, *Adv. Mater.* **2018**, 30, 1706539.
- [9] D. Krapez Tomec, M. Kariz, *Polymers* **2022**, 14, 1174.
- [10] L. Lemetti, J. Tersteegen, J. Sammaljärvi, A. S. Aranko, M. B. Linder, *ACS Sustainable Chem. Eng.* **2022**, 10, 552.
- [11] S. Gong, W. Cui, Q. Zhang, A. Cao, L. Jiang, Q. Cheng, *ACS Nano* **2015**, 9, 11568.
- [12] I. A. Kinloch, J. Suhr, J. Lou, R. J. Young, P. M. Ajayan, *Science* **2018**, 362, 547.
- [13] C. Vepari, D. L. Kaplan, *Prog. Polym. Sci.* **2007**, 32, 991.
- [14] T. J. Deming, *Curr. Opin. Chem. Biol.* **1999**, 3, 100.
- [15] P. Kord Forooshani, B. P. Lee, *J. Polym. Sci. Part Polym. Chem.* **2017**, 55, 9.
- [16] J. H. Waite, X. Qin, *Biochemistry* **2001**, 40, 2887.
- [17] J. H. Waite, *Ann. N. Y. Acad. Sci.* **1999**, 875, 301.
- [18] W. Wei, L. Petrone, Y. Tan, H. Cai, J. N. Israelachvili, A. Miserez, J. H. Waite, *Adv. Funct. Mater.* **2016**, 26, 3496.
- [19] B. Yang, S. Jin, Y. Park, Y. M. Jung, H. J. Cha, *Small* **2018**, 14, 1803377.
- [20] K. Deepankumar, Q. Guo, H. Mohanram, J. Lim, Y. Mu, K. Pervushin, J. Yu, A. Miserez, *Adv. Mater.* **2021**, 34, 2103828.
- [21] W. Wei, Y. Tan, N. R. Martinez Rodriguez, J. Yu, J. N. Israelachvili, J. H. Waite, *Acta Biomater.* **2014**, 10, 1663.
- [22] Q. Lin, D. Gourdon, C. Sun, N. Holten-Andersen, T. H. Anderson, J. H. Waite, J. N. Israelachvili, *Proc. Natl. Acad. Sci. U. S. A.* **2007**, 104, 3782.
- [23] S. A. Mian, L. C. Saha, J. Jang, L. Wang, X. Gao, S. Nagase, *J. Phys. Chem. C* **2010**, 114, 20793.
- [24] M. J. Sever, J. T. Weisser, J. Monahan, S. Srinivasan, J. J. Wilker, *Angew. Chem. – Int. Ed.* **2004**, 43, 448.
- [25] H. Lee, N. F. Scherer, P. B. Messersmith, *Proc. Natl. Acad. Sci.* **2006**, 103, 12999.
- [26] R. J. Stewart, C. S. Wang, H. Shao, *Adv. Colloid Interface Sci.* **2011**, 167, 85.
- [27] Y. Z. Zhou, R. G. Alany, V. Chuang, J. Wen, *Chromatographia* **2012**, 75, 597.
- [28] J. H. Waite, *J. Exp. Biol.* **2017**, 220, 517.
- [29] T. H. Anderson, J. Yu, A. Estrada, M. U. Hammer, J. H. Waite, J. N. Israelachvili, *Adv. Funct. Mater.* **2010**, 20, 4196.
- [30] W. Wei, J. Yu, C. Broomell, J. N. Israelachvili, J. H. Waite, *J. Am. Chem. Soc.* **2013**, 135, 377.
- [31] G. P. Maier, C. M. Bernt, A. Butler, *Biomater. Sci.* **2018**, 6, 332.
- [32] Q. Guo, G. Zou, X. Qian, S. Chen, H. Gao, J. Yu, *Nat. Commun.* **2022**, 13, 5771.
- [33] G. P. Maier, M. V. Rapp, J. H. Waite, J. N. Israelachvili, A. Butler, *Science* **2015**, 349, 628.
- [34] R. J. Stewart, C. S. Wang, H. Shao, *Adv. Colloid Interface Sci.* **2011**, 167, 85.
- [35] S. Y. Bahn, B. H. Jo, Y. S. Choi, H. J. Cha, *Sci. Adv.* **2017**, 3, e1700765.
- [36] Y. Shin, C. P. Brangwynne, *Science* **2017**, 357, aaf4382.
- [37] Y.-H. Lin, J. D. Forman-Kay, H. S. Chan, *Biochemistry* **2018**, 57, 2499.
- [38] P. Batys, D. Fedorov, P. Mohammadi, L. Lemetti, M. B. Linder, M. Sammalkorpi, *Biomacromolecules* **2021**, 22, 690.
- [39] S. Abbott, in *Adhesion Science: Principles and Practice*, Destech Publications, Lancaster, USA, **2015**.
- [40] J. Wang, T. Scheibel, *Biotechnol. J.* **2018**, 13, 1800146.
- [41] K. Marumo, J. H. Waite, *Biochim. Biophys. Acta* **1986**, 872, 98.
- [42] P. Mohammadi, G. Beaune, B. T. Stokke, J. V. I. Timonen, M. B. Linder, *ACS Macro Lett.* **2018**, 7, 1120.
- [43] B. Zakeri, J. O. Fierer, E. Celik, E. C. Chittock, U. Schwarz-Linek, V. T. Moy, M. Howarth, *Proc. Natl. Acad. Sci.* **2012**, 109, E690.
- [44] M. Kitamura, K. Kawakami, N. Nakamura, K. Tsumoto, H. Uchiyama, Y. Ueda, I. Kumagai, T. Nakaya, *J. Polym. Sci. Part Polym. Chem.* **1999**, 37, 729.
- [45] C. D. Lee, H. C. Sun, S.-M. Hu, C. F. Chiu, A. Homhuan, S. M. Liang, C. H. Leng, T. F. Wang, *Protein Sci.* **2008**, 17, 1241.
- [46] J. M. Gosline, P. A. Guerette, C. S. Ortlepp, K. N. Savage, *J. Exp. Biol.* **1999**, 202, 3295.
- [47] A. H. Keeble, A. Banerjee, M. P. Ferla, S. C. Reddington, I. N. A. K. Anuar, M. Howarth, *Angew. Chem., Int. Ed.* **2017**, 56, 16521.
- [48] L. Lemetti, S. P. Hirvonen, D. Fedorov, P. Batys, M. Sammalkorpi, H. Tenhu, M. B. Linder, A. S. Aranko, *Eur. Polym. J.* **2019**, 112, 539.
- [49] P. Mohammadi, A. S. Aranko, C. P. Landowski, O. Ikkala, K. Jaudzems, W. Wagermaier, M. B. Linder, *Sci. Adv.* **2019**, 5, eaaw2541.
- [50] C. P. Brangwynne, T. J. Mitchison, A. A. Hyman, *Proc. Natl. Acad. Sci. U. S. A.* **2011**, 108, 4334.
- [51] J. Eggers, J. R. Lister, H. A. Stone, *J. Fluid Mech.* **1999**, 401, 293.
- [52] A. Y. Xu, L. D. Melton, T. M. Ryan, J. P. Mata, A. Rekas, M. A. K. Williams, D. J. Mcgillivray, *Food Hydrocoll.* **2018**, 77, 952.
- [53] R. O. Ritchie, *Nat. Mater.* **2011**, 10, 817.

- [54] B. L. Smith, T. E. Schäffer, M. Viani, J. B. Thompson, N. A. Frederick, J. Kindt, A. Belcher, G. D. Stucky, D. E. Morse, P. K. Hansma, *Nature* **1999**, 399, 761.
- [55] A. R. Studart, *Adv. Mater.* **2012**, 24, 5024.
- [56] C. Bukowski, T. Zhang, R. A. Riggelman, A. J. Crosby, *Sci. Adv.* **2021**, 7, eabg9763.
- [57] T. P. Niebel, F. Bouville, D. Kokkinis, A. R. Studart, *J. Mech. Phys. Solids* **2016**, 96, 133.
- [58] E. W. Danner, Y. Kan, M. U. Hammer, J. N. Israelachvili, J. H. Waite, *Biochemistry* **2012**, 51, 6511.
- [59] H. Lee, N. F. Scherer, P. B. Messersmith, *Proc. Natl. Acad. Sci.* **2006**, 103, 12999.
- [60] T. H. Anderson, J. Yu, A. Estrada, M. U. Hammer, J. H. Waite, J. N. Israelachvili, *Adv. Funct. Mater.* **2010**, 20, 4196.
- [61] M. J. Brennan, B. F. Kilbride, J. J. Wilker, J. C. Liu, *Biomaterials* **2017**, 124, 116.
- [62] J. Yu, W. Wei, E. Danner, R. K. Ashley, J. N. Israelachvili, J. H. Waite, *Nat. Chem. Biol.* **2011**, 7, 588.
- [63] D. S. Hwang, H. Zeng, Q. Lu, J. Israelachvili, J. H. Waite, *Soft Matter* **2012**, 8, 5640.
- [64] D. S. Hwang, H. Zeng, A. Srivastava, D. V. Krogstad, M. Tirrell, J. N. Israelachvili, J. H. Waite, *Soft Matter* **2010**, 6, 3232.
- [65] D. R. Miller, S. Das, K. Y. Huang, S. Han, J. N. Israelachvili, J. H. Waite, *ACS Biomater. Sci. Eng.* **2015**, 1, 1121.
- [66] W. Wei, L. Petrone, Y. Tan, H. Cai, J. N. Israelachvili, A. Miserez, J. H. Waite, *Adv. Funct. Mater.* **2016**, 26, 3496.
- [67] M. A. Morando, F. Venturella, M. Sollazzo, E. Monaca, R. Sabbatella, V. Vetri, R. Passantino, A. Pastore, C. Alfano, *Commun. Biol.* **2022**, 5, 739.
- [68] L. Petrone, A. Kumar, C. N. Sutanto, N. J. Patil, S. Kannan, A. Palaniappan, S. Amini, B. Zappone, C. Verma, A. Miserez, *Nat. Commun.* **2015**, 6, 8737.
- [69] K. Kendall, in *Molecular Adhesion and Its Applications*, Kluwer Academic Publishers, Boston, **2004**.
- [70] R. V. Pappu, S. R. Cohen, F. Dar, M. Farag, M. Kar, *Chem. Rev.* **2023**, 123, 8945.
- [71] Y. Shen, F. S. Ruggeri, D. Vigolo, A. Kamada, S. Qamar, A. Levin, C. Iserman, S. Alberti, P. S. George-Hyslop, T. P. J. Knowles, *Nat. Nanotechnol.* **2020**, 15, 841.
- [72] P. Mohammadi, A. S. Aranko, L. Lemetti, Z. Cenev, Q. Zhou, S. Virtanen, C. P. Landowski, M. Penttilä, W. J. Fischer, W. Wagermaier, M. B. Linder, *Commun. Biol.* **2018**, 1, 86.
- [73] J. Hong, Q. Lin, Z. Shao, *ACS Macro Lett.* **2023**, 12, 888.
- [74] F. L. Leite, P. S. P. Herrmann, *J. Adhes. Sci. Technol.* **2005**, 19, 365.
- [75] C. A. Helm, W. Knoll, J. N. Israelachvili, *Proc. Natl. Acad. Sci. USA* **1991**, 88, 8169.
- [76] K. L. Johnson, K. Kendall, A. D. Roberts, *Proc. R. Soc. Lond. Math. Phys. Sci.* **1971**, 324, 301.
- [77] J. Sprakel, N. A. M. Besseling, M. A. Cohen Stuart, F. A. M. Leermakers, *Langmuir* **2008**, 24, 1308.
- [78] E. Spruijt, J. Sprakel, M. A. Cohen Stuart, J. Van Der Gucht, *Soft Matter* **2010**, 6, 172.